2023-08-21

Enhanced Capabilities for Investigating Local Structure and Magnetism: Three Dimensional Magnetic Pair Distribution Function and Symmetry Mode Analysis

Parker Hamilton
Brigham Young University

Enhanced Capabilities for Investigating Local Structure and Magnetism:

Three Dimensional Magnetic Pair Distribution Function

and Symmetry Mode Analysis

Parker Hamilton

A thesis submitted to the faculty of
Brigham Young University
in partial fulfillment of the requirements for the degree of

Master of Science

Benjamin Frandsen, Chair
Branton Campbell
Dennis Della Corte

Department of Physics and Astronomy

Brigham Young University

ABSTRACT

Enhanced Capabilities for Investigating Local Structure and Magnetism:
Three Dimensional Magnetic Pair Distribution Function
and Symmetry Mode Analysis

Parker Hamilton
Department of Physics and Astronomy, BYU
Master of Science

The local structure, atomic and magnetic structure correlated over a small length scale, of a material has a strong impact on material properties. Pair distribution function (PDF) analysis is a strong tool to investigate local structure and magnetism of this nature. This work outlines extensions to current one dimensional magnetic pair distribution functions (1D-mPDF) and the fitting of structures with symmetry breaking local atomic distortions. 1DmPDF analysis has been used to study local magnetic structure, but requires a rotational averaging of the correlations so directional information is lost, as in powder diffraction experiments. Three dimensional difference magnetic pair distribution function (3D-ΔmPDF) analysis does not require this rotational averaging and preserves directional information. This is a useful tool in analyzing experimental data like single crystal neutron diffraction and studying locally anisoptropic magnetic structures. Here we present a technique and software tools to calculate the 3D-ΔmPDF pattern of a given structure and give a brief analysis of the local magnetic structure of MnTe. Another problem in PDF analysis is the modeling of structures with symmetry breaking local atomic distortions. Symmetry-adapted distortion modes have been used for structural refinement in Rietveld refinement for at least 10 years; more more recently, this has also been applied to PDF data. We present here a detailed discussion of the use of symmetry-adapted modes for structural refinement using PDF data. We also outline new open-sourced software tools to apply this technique and show two analyses using symmetry-adapted structural modes.

Keywords: total scattering, pair distribution function, PDF, magnetic structure, distorted structure, symmetry modes, local structure

ACKNOWLEDGMENTS

I would like to thank my advisor Ben Frandsen for the mentorship, patience, and constant feedback that made this work possible. I would also like to acknowledge the support of my family, especially my wife in helping me through the personal aspects of graduate work.

Contents

Chapter 1

Structure and Crystallography

1.1 Introduction

Advanced technology increasingly demands advanced materials with improved performance and novel behaviors. Diffraction techniques are a long-standing tool for the characterization of the atomic level structure of materials and the investigation of structure-property relationships. In many cases, the material properties of interest are strongly influenced by the local structure, which refers to the structural correlations that exist on short length scales (e.g., nanometer or sub-nanometer scales). The local structure can often deviate substantially from the long-range structure; for example, a collective displacement of atoms that is correlated over a few unit cells may be uncorrelated (and hence average to zero) over longer length scales. Traditional material structure analysis focuses on the long-range structure encoded in the Bragg peaks in a diffraction pattern, typically ignoring the diffuse scattering that contains information about short-range correlations [1]. While understanding long-range structure is essential in materials discovery, traditional approaches are not sensitive to local structure deviations and therefore fail to characterize material structure accurately on the nanoscale [2, 3].

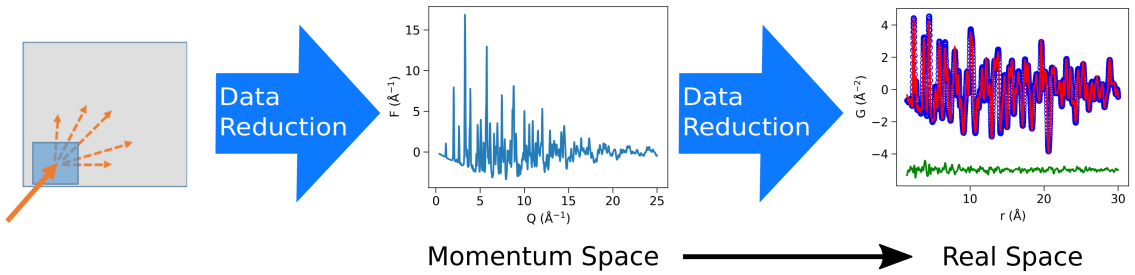

Figure 1.1 PDF analysis of diffraction data is performed by taking a Fourier transform of the total scattering. The resulting PDF pattern is a real-space quasi correlation function.

Pair distribution function (PDF) analysis, illustrated in Fig. 1.1, provides an alternative approach to analyzing diffraction data that offers sensitivity to features of the local structure. Instead of using traditional Bragg peak analysis in momentum space, PDF analysis makes use of the total scattering, i.e., both Bragg and diffuse scattering, and Fourier transforms it into real space to yield a correlation function [1]. This real-space correlation function is comprised of the pairwise atomic correlations that define the local structure [4]. The goal of PDF analysis is then to quantitatively

probe the structure of the sample on local length scales. The most common way this is done is to compute the PDF of a proposed theoretical structure, compare it to experimentally measured data, and iteratively fit the theoretical structure to the experimental data set. Similar to traditional Rietveld refinement [5, 6], the structural parameters that can be optimized include the dimension of the unit cell, the positions of the atoms within the unit call, the vibrational amplitudes of the atoms around their equilibrium positions, and more. PDF differs from diffraction analysis in that the fits are optimized to real-space PDF data over typical distances of 2-3 nm, as opposed to probing correlations over hundreds or thousands of nanometers typical for Bragg diffraction analysis. PDF models can be fit over a longer r range, but are ultimately limited by the resolution of the instruments being used.

PDF techniques are widely applicable and have been used in the structural analysis of crystals, molecular matter, magnetic structures, and amorphous materials. A few examples of atomic PDF analysis are investigating negative thermal expansion, where a materials will contract as it heats, ferroelectrics, spin glasses and spin ices, and nanoparticles [7]. It has also been used to model molecular matter such as organic polymers, non graphitic carbon structures, and pharmaceuticals [8] as more not mentioned here. The following work details advances in PDF analysis in two specific areas: analyzing magnetic structures, and modeling local distortions leading to disorder. Also included in this work are a set of open source software tools developed and published to assist researchers in using the PDF methods developed in the present work.

1.2 Outline of This Thesis

The following chapters will start with an outline of the current state of the art for both magnetic PDF and modeling distortions of the local structure in Chapter 2. Also in that chapter will be a short description of how this works adds to both of the previously mentioned areas. Chapter 3 and Chapter 4 will give in depth descriptions of the approaches taken for magnetic PDF modeling and local structure modeling respectively. Both chapters include example analyses using the techniques

discussed here in this work. The last chapter is a brief summary and discussion of the the work presented here.

Much of the research presented here is included in three different papers I have been involved in. The first is an analysis of the magnetic local structure of MnTe using neutron diffraction [9]. This project presents both one dimensional (1D-mPDF) and three dimensional difference magnetic PDF (3D-ΔmPDF) data on short-range magnetic correlations in MnTe that enhance the thermoelectric properties of this material. I led the modeling of the 3D-ΔmPDF seen in the supplemental material and fit the spin correlation lengths discussed in the paper. The second paper is a detailed description of the `diffpy.mpdf` open sourced software package for magnetic pair distribution function analysis [10]. The package includes tools for calculating the 1D-mPDF and 3D-ΔmPDF patterns. I wrote and tested the software tools for the 3D-ΔmPDF and contributed to the magnetic structure representation by developing a mathematical model for spatially anisotropic spin correlation lengths. I also worite the associated sections in the paper. Lastly, I wrote a first author paper on our approach to local structure modeling [11]. This paper is under review at *J. Appl. Cryst.*, the preprint posted on arXiv is cited here. I was the primary researcher on this project and wrote the associated software tools and performed the analyses described later in Chapter 4.

Chapter 2

Advancing Pair Distribution Function Analysis

2.1 Magnetic PDF

The vast majority of PDF work to date has focused on determining the local atomic structure, i.e. the arrangement of the atoms in a material [12]. Recently, however, the magnetic pair distribution function (mPDF) has been introduced as a new way to probe short-range magnetic correlations in magnetic materials [13, 14]. Magnetic PDF (mPDF) follows the same principles as atomic PDF, except that it is applied to the magnetic scattering cross section of neutrons incident on a material with nonzero magnetic moments. The nature of magnetic scattering differs from nuclear scattering because it involves a spin-spin interaction, which is an interaction between two vectors, so the scattering cross section is correspondingly more complex. The mPDF is likewise more complex than the atomic PDF, but the primary intuition as a real-space correlation function between pairs of spins remains in place. To date, mPDF has been applied to a variety of magnetic materials in powder samples, demonstrating its feasibility and efficacy [15].

A weakness of one dimensional PDF techniques is the rotational averaging that is necessary when measuring poly-crystalline samples. This superimposes information at equal distances and so both weak distortions and anisotropic structure can be lost. The three-dimensional difference PDF (3D-ΔPDF) has two unique features from the normal 1D PDF, the separation of spatial directions and the inclusion of only the disorder, not the average structure. The inclusion of only the disorder is a way to view weak distortions from the average structure and the separation of directions can show directionally dependent features of the local disorder that might not have been seen otherwise.

The 3D-ΔmPDF was initially developed for atomic correlations but the theory has been extended by Roth et.al. [16] to magnetic spin correlations as well. No software tools for calculating the 3D-ΔmPDF have previously been developed that are available to the general research community. Here the 3D-ΔmPDF is implemented based on the work of Roth et.al. in the open sourced python package `diffpy.mpdf` and used to investigate anisotropic local magnetic structure in MnTe.

2.2 Modeling Local Structure

A typical objective of PDF analysis is to identify and characterize symmetry-breaking distortions in the local structure that average to zero over longer length scales. Local symmetry breaking of this type can provide crucial information about the underlying physics of the material under investigation [2, 3, 7, 17–21]. In the commonly used "small-box modeling" or "real-space Rietveld" approach, one often starts with fitting a high-symmetry average-structural model to the low-r portion of the data, and looks for systematic misfits that provide evidence for and information about any short-range structural distortions. The next step is then typically to test lower-symmetry models against the a low r data to see if the fit improves, and if so, attempt to determine what physical insights can be gained from the lower-symmetry model.

Two commonly occurring obstacles can make this strategy difficult. First, selecting candidate lower-symmetry models can often be an *ad hoc* process requiring tedious guesswork by the PDF analyst, and even if some distorted model that improves the fit is identified, it may not be clear whether other distorted models could provide equally good or even better fits. Second, lower-symmetry models will naturally have a greater number of free parameters (e.g. atomic positions and atomic displacement parameters [ADPs]) to be optimized in the fit, which can impede the optimization routine from converging reliably.

These difficulties apply both to PDF and Rietveld analysis of diffraction data. A promising way to overcome these challenges is to use a symmetry-adapted fitting scheme using the tools of group theory, as has been demonstrated for Rietveld refinements with diffraction data [22, 23]. Using software such as ISODISTORT [24], one can start with a parent structure and systematically explore distorted child structures down to arbitrarily low symmetry and up to an arbitrarily large supercell. Comparing the fit results allows one to build a more complete picture of potential distorted structures that could explain the data. This addresses the first of the previously mentioned challenges. In addition, one can define as fit variables the amplitudes of the symmetry modes allowed for a given structure, in place of the atomic coordinates for individual atoms that are conventionally used as fit variables. A single variable in the form of a mode amplitude may therefore control the collective

motion of several distinct atoms. Because structural distortions often correspond to a small number of symmetry modes taking nonzero amplitudes, the use of symmetry mode amplitudes as a basis for the fit variables can greatly reduce the number of variables required to achieve a good fit, leading to more robust convergence. In addition, the symmetry modes relevant for a given structural distortion can be identified directly from the fit, providing greater clarity to the physical interpretation of the fit results. This feature of a symmetry-adapted fitting scheme addresses the second of the challenges mentioned previously.

Recently, symmetry-mode analysis has been applied to PDF data [25]. Bird *et al.* introduced a procedure for refining distortion mode amplitudes from PDF data that entails (1) downloading the symmetry mode information from the ISODISTORT web application, (2) running a script to convert the output into a format that can be read by the commercial structural refinement software TOPAS-Academic [26], and (3) iterating through a series of refinements in TOPAS to identify and evaluate candidate distortion modes. The approach was successfully used to characterize dynamic distortions in the negative thermal expansion material ScF_3 and short-range distortions in the prototypical ferroelectric $BaTiO_3$, demonstrating that a symmetry-adapted fitting scheme can be applied to PDF analysis, providing the aforementioned advantages over conventional fitting methods. Additionally, this impact will be amplified by providing open sourced software tools for automatable, high throughput fit execution as well as a flexible, scriptable python interface for accessing the ISODISTORT web application removing the manual aspect of the work flow.

Chapter 3

Advancing 3D-ΔmPDF: Software Development and Application to MnTe

3.1 Introduction

Magnetic pair distribution function (mPDF) analysis of neutron total scattering data was introduced in 2014 as a method for studying local magnetic correlations in materials [27]. Analogous to the more familiar atomic pair distribution function (PDF) method [28], mPDF analysis utilizes the Fourier transform of the magnetic neutron scattering cross section to yield information about pairwise magnetic correlations in real space. The method can be used for both powder samples and single crystals [16], the latter case yielding the three-dimensional difference magnetic pair distribution function (3D-ΔmPDF). Magnetic PDF analysis has been successfully applied to the study of long- and short-range magnetic correlations in numerous magnetic systems, including strongly correlated electron systems [15, 29, 30], geometrically frustrated magnets [31–34], spin glass systems [35], technologically relevant ferromagnets and antiferromagnets [9, 36, 37], and others [38]. Here, we present the 3D-ΔmPDF capabilities built into `diffpy.mpdf`, the first full-featured, open-access software package for mPDF analysis.

3.2 Theoretical Background

The 3D-ΔmPDF is a measure of correlated magnetic disorder in a single crystal [16], analogous to the 3D-ΔPDF for correlated atomic disorder [39]. The 3D-ΔmPDF is obtained via the Fourier transform of the diffuse magnetic scattering, thereby differing from standard PDF techniques where both Bragg and diffuse scattering are included. As such, the 3D-ΔmPDF is sensitive specifically to deviations from the average magnetic structure. In a system without long-range magnetic order, such as a magnetic material above the ordering temperature, there is no average magnetic structure, so the 3D-ΔmPDF reflects all magnetic correlations present. Compared to powder samples, single crystals offer a more feasible route to separating the diffuse scattering from Bragg scattering through methods such as punch and fill [39], KAREN [40], or temperature subtraction.

For a given magnetic structure, the 3D-ΔmPDF is given by [16]

$$\text{3D-}\Delta\text{mPDF}(\mathbf{r}) = \mathscr{F}^{-1}\left[\frac{d\sigma_{\text{Diffuse}}}{d\Omega}\right] \tag{3.1}$$

$$= \frac{r_0^2}{4\mu_B^2}\langle \delta\mathbf{M} \bar{\otimes} \delta\mathbf{M} - \frac{1}{\pi^4}(\delta\mathbf{M} \bar{*} \Upsilon) \otimes (\delta\mathbf{M} \bar{*} \Upsilon)\rangle, \tag{3.2}$$

where the derivative in equation 3.1 is the differential scattering cross section of only the diffuse scattering, the independent variable $\mathbf{r}$ is the vector separating two points in real space (e.g. the separation vector between two magnetic moments), $\delta\mathbf{M}$ is the vector field describing the local deviations from the average magnetic structure as a function of $\mathbf{r}$, r_0 is the classical electron radius as before, and μ_B is the Bohr magneton. Υ arises from the vector interaction of the neutron spin and the electronic magnetic moments in the material and is defined as

$$\Upsilon \equiv \begin{cases} \frac{\mathbf{r}}{|r|^4}, & r \neq 0 \\ \mathbf{0}, & r = 0 \end{cases}. \tag{3.3}$$

The vector-field cross correlation and convolution operators ($\bar{\otimes}$ and $\bar{*}$) are defined for two vector fields $\mathbf{f}$ and $\mathbf{g}$ as

$$\mathbf{f} \bar{\otimes} \mathbf{g} \equiv f_1 \otimes g_1 + f_2 \otimes g_2 + f_3 \otimes g_3 \tag{3.4}$$

$$\mathbf{f} \bar{*} \mathbf{g} \equiv f_1 * g_1 + f_2 * g_2 + f_3 * g_3, \tag{3.5}$$

where f_i, g_i are the scalar functions comprising the i^{th} component of the corresponding vector field and $\otimes$ and $*$ are the usual scalar cross-correlation and convolution operators, respectively. It can be seen from (3.2) that the 3D-ΔmPDF can be thought of as an auto-correlation of the local magnetization with an additional term to account for the complexity that arises from neutron scattering from a vector magnetization density rather than a scalar density.

The new capability presented by the 3D-ΔmPDF method to capture the directional dependence of the magnetic spin correlations, which is largely lost in the rotational averaging of the 1D-mPDF, allows for the analysis of aniostropic spin correlation lengths. This requires the development of a new mathematical method to represent these directionally dependent correlations. We represent an anistropic correlation length using an ellipsoid, where the distance from the center to the surface

of the ellipsoid in any given direction is the correlation length in that direction. The surface of an ellipsoid is described by the equation

$$x^T D x = 1, \tag{3.6}$$

where x is the three-component Cartesian vector from the center of the ellipsoid to an arbitrary point on the surface of the ellipsoid and D is a symmetric matrix of the form

$$D = \begin{bmatrix} D_{11} & \frac{1}{2}D_{12} & \frac{1}{2}D_{13} \\ \frac{1}{2}D_{12} & D_{22} & \frac{1}{2}D_{23} \\ \frac{1}{2}D_{13} & \frac{1}{2}D_{23} & D_{33} \end{bmatrix}. \tag{3.7}$$

If we consider an arbitrary direction denoted by the unit vector $\hat{n}$, we can determine the correlation length ξ along that direction by substituting the vector $\xi\hat{n}$ for x in Eq. 3.6, yielding the desired equation for ξ

$$\xi = (\hat{n}^T D \hat{n})^{-\frac{1}{2}}. \tag{3.8}$$

Thus, one can implement any desired ellipsoidal correlation length by constructing a suitable D matrix. Because the components of D are related to the rate at which magnetic correlations decay along certain directions, we call D the damping matrix.

The eigenvectors of D represent the principal axes of the correlation ellipsoid, while the eigenvalues are the inverse square of the correlation length along each of the principal axes. If physical considerations suggest a certain set of principal axes for the correlation ellipsoid, then we can use these principal axes and their associated correlation lengths to construct D through spectral decomposition:

$$D = V \Lambda V^T \tag{3.9}$$

$$= [n_1, n_2, n_3] \begin{bmatrix} \frac{1}{\xi_1^2} & 0 & 0 \\ 0 & \frac{1}{\xi_2^2} & 0 \\ 0 & 0 & \frac{1}{\xi_3^2} \end{bmatrix} \begin{bmatrix} n_1^T \\ n_2^T \\ n_3^T \end{bmatrix}. \tag{3.10}$$

The `diffpy.mpdf` package allows users to construct the damping matrix directly or by providing a set of orthornormal eigenvectors (i.e., the directions of the principal axes of the ellipsoid) and their

correlation lengths.

3.3 The diffpy.mpdf Software

The diffpy.mpdf software package is an open source set of software tools for calculating magnetic PDF patterns and fitting structural models to mPDF data. The package is written in python and the primary class element is the MagStructure object, which contains information about the positions, orientations, and magnetic moments of a theoretical material structure. The package also has two calculators, on for 1D-mPDF and one for 3D-ΔmPDF. Both utilize just the MagStructure class to calculate their respective mPDF patterns as the mPDf can be primarily thought of as a spin-spin correlation function.

3.4 Calculating the 3D-ΔmPDF

The 3D-ΔmPDF is calculated by evaluating Eq. 3.2 for a given set of magnetic moment vectors and position vectors representing the magnetic structure. We convolve each position vector with a user-specifiable 3D Gaussian function, approximating the effect of the finite spatial extent of the wave functions of the unpaired electron(s) giving rise to each magnetic moment. The user can also specify the 3D real-space grid on which the 3D-ΔmPDF is to be evaluated. The code to compute the 3D-ΔmPDF, some of which is shown in Fig. 3.1, makes heavy use of the convolution and correlation functions from the scipy signal processing library. While these functions are highly optimized, the number of grid points scales cubically with incresing system size and real-space resolution. For the example given below computation of the 3D-ΔmPDF was on the order of minutes. An additional aspect of the code base for the 3D-ΔmPDF is a set of visualization aids to assist in generating arbitrary slices of the 3D data to navigate different directions and planes of the 3D-ΔmPDF pattern.

```
125         filter_x = np.arange(-3,3+self.dr,self.dr)
126         X,Y,Z = np.meshgrid(filter_x,filter_x,filter_x,indexing='ij')
127         filter_grid = np.moveaxis([X,Y,Z],0,-1)
128
129         if verbose:
130             print("Making filters")
131
132         gaussian = gauss(filter_grid,s=self.gaussPeakWidth)
133         upsilon = ups(filter_grid)
134
135         if verbose:
136             print("Convolving spin array")
137
138         s_arr[:,:,:,0] = sig.convolve(s_arr[:,:,:,0],gaussian,mode='same')*self.dr**3
139         s_arr[:,:,:,1] = sig.convolve(s_arr[:,:,:,1],gaussian,mode='same')*self.dr**3
140         s_arr[:,:,:,2] = sig.convolve(s_arr[:,:,:,2],gaussian,mode='same')*self.dr**3
141
142         if verbose:
143             print("Computing mpdf")
144
145         mag_ups = vec_con(s_arr,upsilon,self.dr)
146         self.mpdf = vec_ac(s_arr,s_arr,self.dr,"full")
147         self.mpdf += -1/(np.pi**4)*sig.correlate(mag_ups,mag_ups,mode="full")*self.dr**3
148
149         return
```

Figure 3.1 The main lines of code from `diffpy.mpf` for calculating the 3D-ΔmPDF. Lines 145-147 reference the vector convolution and vector auto-correlation functions defined previously.

3.4.1 Example

We present the 3D-ΔmPDF of the antiferromagnetic semiconductor MnTe as an example case. MnTe has a hexagonal crystal structure and orders magnetically below $T_N = 307$ K, with the moments aligned ferromagnetically within the *ab* plane and antiferromagnetically along the *c* axis [41]. Short-range antiferromagnetic correlations are known to persist to high temperatures well into the paramagnetic phase [9, 42].

In Fig. 3.2(a), we show the $z = 0$ plane of the calculated 3D-ΔmPDF for MnTe in the correlated paramagnet regime above T_N. The magnetic configuration was generated using experimentally verified *ab initio* calculations [9]. In the plots, red is a positive correlation/ferromagnetic alignment and blue is a negative correlation/antiferromagnetic alignment. The hexagonal structure and ferromagnetic alignment within the plane can both be seen. In Fig. 3.2(b), we show the $y = 0$ slice of the same calculation, providing a view of the out-of-plane correlations. The horizontal rows of alternating red and blue spots illustrate the antiferromagnetic correlations along the z axis. We also

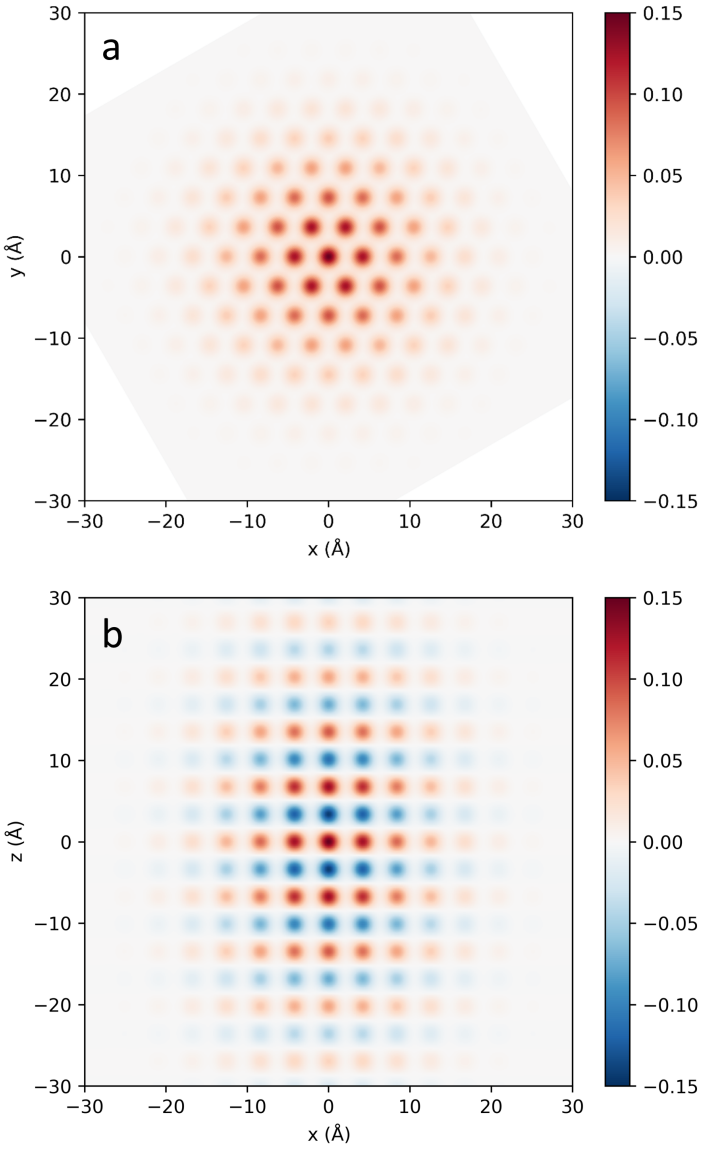

Figure 3.2 (a) The $z = 0$ plane of the calculated 3D-ΔmPDF pattern for MnTe above T_N. The calculation shows short-range ferromagnetic correlations in the xy plane. (b) The $y = 0$ plane of the calculated 3D-ΔmPDF pattern for MnTe above T_N. The calculation shows short-range antiferromagnetic correlations in the z direction. The units shown in the color bar for both panels are arbitrary, but the sign is significant: for a given separation vector, a positive (negative) value of the 3D-ΔmPDF indicates greater parallel (antiparallel) alignment of the magnetization relative to the average magnetic structure. In the present case of a correlated paramagnet, there is no average magnetic structure, so the 3D-ΔmPDF shows the local magnetic correlations directly.

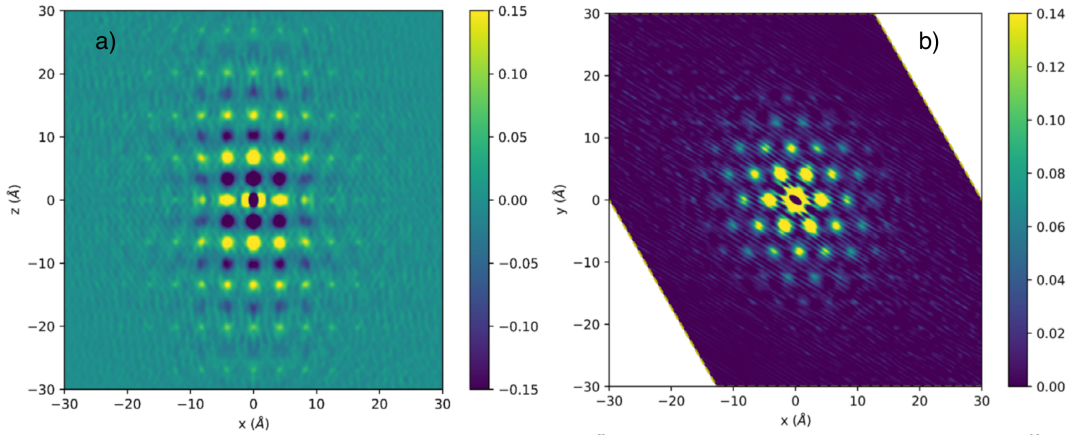

Figure 3.3 Experimental 3D-ΔmPDF patterns from MnTe taken above the magnetic transition temperature, showing surviving local correlations. This data was taken by Raju Baral and analysed by Jacob Christensen [43]. (a) The z=0 plane of the experimental 3D-ΔmPDF. (b) The y=0 plane of the experimental 3D-ΔmPDF. In the above images yellow indicates a positive ferromagnetic correlation and blue is a negative antiferromagnetic correlation.

note the strikingly anisotropic correlation length, which is significantly longer along z than within the xy plane. This originates from the disparate strengths of the magnetic exchange interactions [9]. Fig. 3.3 shows experimental of the 3D-ΔmPDF for MnTe. The data was taken by Raju Baral and the analysis was done by Jacob Christensne [43]. Comparing Figures 3.2 and 3.3, we can see very good agreement between the measured experimental data and the simulated 3D-ΔmPDF. The one feature not accounted for is a slight butterfly envelope seen in Fig. 3.3a that we were unable to model.

3.5 Availability and resources

The `diffpy.mpdf` package is open source and distributed under the 3-Clause BSD license. The source code is freely available to download and install at https://github.com/FrandsenGroup/diffpy.mpdf. The software runs on Linux and Macintosh operating systems and the Windows Subsystem for Linux. Tutorial files in the form of Jupyter Notebooks and python scripts are also available at the same website to demonstrate important functionalities, including generating magnetic structure descriptions, calculating one- and three-dimensional mPDF patterns, performing fits to data, and a

selection of more advanced usage cases.

For this portion of the work we thank Caleb Dame for valuable contributions to the interactive magnetic structure builder and Matthew Richards for help with the fitting algorithms. Work by B.A.F. and P.H. was supported by the U.S. Department of Energy, Office of Science, Office of Basic Energy Sciences (DOE-BES) through Award No. DE-SC0021134. J.A.C. and E.S. acknowledge support from the College of Physical and Mathematical Sciences at Brigham Young University. S.J.L.B. was supported by U.S. Department of Energy, Office of Science, Office of Basic Energy Sciences (DOE-BES) under contract No. DE-SC0012704. This study used resources at the Spallation Neutron Source (SNS), a DOE Office of Science User Facility operated by the Oak Ridge National Laboratory

Chapter 4

Symmetry mode PDF analysis

4.1 Introduction

Here, we explain the details of symmetry-adapted PDF analysis, demonstrate the value of the approach, and introduce new software tools for implementing this approach in an automatable, fully open-source way. We have developed the open-source python packages `pydistort` and `isotools`, which respectively enable automatic calls to ISODISTORT from a python script and convert the ISODISTORT output into a format suitable for structural refinements using the open-source DiffPy library [44]. This work broadens the impact of symmetry-adapted PDF analysis by eliminating exclusive reliance on commercial software and making possible high throughput analysis. We use this method to study two complementary examples drawn from materials of significant recent interest: the charge-density-wave (CDW) compound $TiSe_2$, which displays a long-range but subtle structural distortion, and the high-performance thermoelectric candidate MnTe, where we observe a large but highly localized distortion. In both cases, we identify the relevant distortions and achieve excellent PDF fits through a systematic and automated exploration of all possible symmetry modes. The results further emphasize the advantages of using symmetry modes when performing structural refinements and suggest that the open-source tools introduced here can be successfully applied to a wide variety of materials.

4.2 Methodology: Refining distortion models using symmetry modes

A symmetry-breaking distortion removes certain symmetry elements of the parent space group. The remaining symmetry elements that persist in the distorted structure comprise the "distortion symmetry" or "isotropy subgroup" which is also the space group of the distorted structure. In this work, we consider only displacive distortions involving changes in the positions of the atoms. To test distorted structural models against PDF data, we use ISODISTORT, which can generate all possible distortion symmetries of a given parent structure for a user-specified supercell and space-group type.

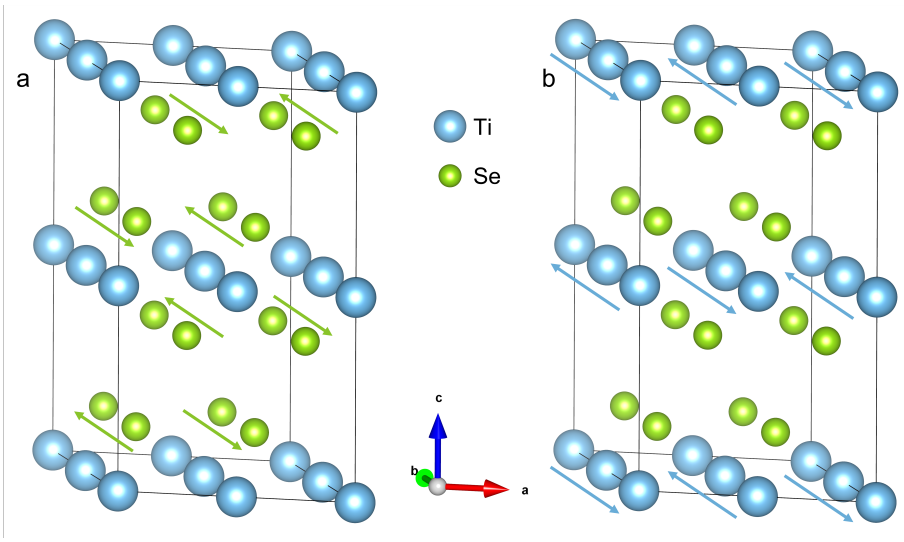

Figure 4.1 A $2 \times 2 \times 2$ supercell of the $P\bar{3}m1$ structure of $TiSe_2$, visualized using VESTA [45]. The arrows depict distortions belonging to the L_1^- irrep. (a) The Se distortion corresponding to the $E(c)$ mode. (b) The Ti distortion corresponding to the $E_u(c)$ mode.

Furthermore, ISODISTORT can express the distortion models using either the traditional *xyz* basis of atomic coordinates or the symmetry-adapted basis of symmetry mode amplitudes.Symmetry modes are basis vectors of the irreducible matrix representations (irreps) of the parent symmetry group, and therefore provide a complete and orthogonal basis of distortion space. For a given distortion symmetry, these two bases—the *xyz* basis and the mode-amplitude basis—are related by a linear transformation calculated by ISODISTORT. In general, a single mode amplitude can affect the positions of multiple atoms, and the displacement of a single atom may be affected by the amplitudes of multiple modes. Since both bases describe the same distortion space, the number of symmetry modes always equals the number of independent atomic coordinates. For $P1$ symmetry, there are no constraints on atomic positions, so that for a supercell with N atoms, there are $3N$ atomic coordinates and $3N$ symmetry modes. For higher symmetries, of course, there will be fewer degrees of freedom, since not all atomic displacements will be independent. An example of a symmetry mode from the $TiSe_2$ study described later is shown in Fig. 4.1.

The traditional approach to refining a distorted structural model is to use the *xyz* coordinates as fitting variables and refine the positions of the atoms directly. However, if the correct distortion

symmetry is not known (and sometimes even if it is), there may be so many degrees of freedom that standard fitting algorithms have difficulty converging to a good result. Recognizing that distortions are often dominated by one or a few modes while the others remain inactive, it can be much more effective to use mode amplitudes as fit variables rather than atomic coordinates [22]. A small number of free parameters corresponding to the mode amplitudes can therefore capture collective displacements of multiple atoms that would otherwise require a larger number of atomic coordinates to describe, effectively reducing the size of the relevant parameter space. Furthermore, the fitting scheme can be organized such that one symmetry mode is tested at a time while all the others remain fixed, which allows the identification of relevant modes much more effectively than would be possible by cycling through the individual atomic coordinates. Finally, this symmetry-informed approach directly reveals which symmetry modes are active in a given structure, yielding insight into the underlying physics at play in the material.

In this work, we use original open-source python packages `pydistort`, which interfaces directly with the ISODISTORT server online through a python script inspired by similar functionality available in GSAS-II [46], and `isotools`, which converts the ISODISTORT output into a format compatible with the open-source DiffPy suite for PDF fitting and analysis. These developments remove the need to manually click through the ISODISTORT web interface to generate the distortion models, providing a significantly greater degree of automation and flexibility when performing symmetry-mode fits to PDF data, all within a fully open-source software environment. Below we describe the typical workflow, which can be carried out completely within a python script or jupyter notebook using the functions defined in our python packages.

1. Upload a crystallographic information file (CIF) corresponding to the parent structure (e.g. as determined by Rietveld refinements to diffraction data or by PDF fits conducted over a long fitting range) to the ISODISTORT server, together with an optional dictionary of ISODISTORT arguments such as the lattice basis of the supercell relative to the parent cell or the desired space group of the child structure ($P1$ by default). This is done with the `pydistort` package. The code interfacing with ISODISTORT then automatically works

through the steps to produce a human-readable file (in TOPAS format) containing all the symmetry modes compatible with the specified supercell and space group. This file is automatically downloaded from the ISODISTORT server. Other ISODISTORT output files can also be requested by the user, such as a CIF or interactive distortion visualization file. Note that ISODISTORT uses the irrep naming conventions of Cracknell, Davies, Miller, and Love (CDML) [47]

2. Create a DiffPy-compatible structure object from the ISODISTORT output using the `isotools` package.

3. Input the symmetry-mode amplitudes as variables to be optimized in the fit, together with the usual fit variables such as a scale parameter, lattice parameters, and ADPs. The `isotools` package automatically implements the appropriate constraints relating the mode amplitudes to the atomic coordinates based on the ISODISTORT output.

4. Use `diffpy.srfit` to carry out the fit however the user desires. For example, the user can cycle through each mode amplitude individually, refine multiple amplitudes in arbitrarily defined groups, perform multiple fits with random starting values, impose a cost for activating additional modes [22], establish a threshold for improvement in the fit quality to consider a mode active [25], etc.

5. Modify the `diffpy.srfit` script as desired for automatic batch fits to multiple data sets, different fitting ranges, etc.

We followed this basic workflow to study distortions present in $TiSe_2$ and MnTe.

4.3 Experimental details

A powder sample of $TiSe_2$ was synthesized via solid state reaction by our collaborator Jaime Moya at Rice University. Powdered Ti and Se were weighed out in the atomic ratio of Ti:Se 1:2.02 and

ground together in accordance with Ref. [48]. The resultant powder was sealed in a quartz tube under ∼3 Torr of partial argon atmosphere and heated at a rate of 50 °C/hr to 650 °C. The sample remained at 650 °C for 48 hours before being quenched to ambient temperature.

The powder sample of MnTe was the same one used in Ref. [9]. It was prepared by thoroughly mixing stoichiometric amounts of Mn powder and Te pieces in an argon glove box, sealing the mixture in an evacuated quartz tube, and placing it in a furnace at 950 °C for 6 hours. The ampoule was then quenched in ice water and annealed further at 650 °C for 72 hours. A mortar and pestle were used to grind the sample into a fine powder in the glove box.

The x-ray total scattering experiments were performed at the National Synchrotron Light Source II (NSLS-II) at Brookhaven National Laboratory on beamline 28-ID-1. The incident wavelength was 0.167 Å. Finely ground powder samples were loaded into thin kapton capillaries sealed with clay. A large amorphous silicon area detector was used to record the diffraction patterns, which were azimuthally integrated using DIOPTAS [49]. The resulting one-dimensional diffraction patterns were normalized and Fourier transformed with $Q_{\max} = 25$ Å^{-1} to produce the PDF using the xPDFsuite program [50].

The neutron total scattering experiments were performed at the Nanoscale-Ordered Material Diffractometer (NOMAD) at the Spallation Neutron Source (SNS) of Oak Ridge National Laboratory (ORNL) [51]. The powder samples were loaded in quartz capillaries and mounted in the beam. Neutron scattering data were collected for an integrated proton current of 4 C and then reduced and transformed with $Q_{\max} = 25$ Å^{-1} using ADDIE [52], the automatic data reduction program at NOMAD.

4.4 Results

4.4.1 $TiSe_2$

The transition-metal dichalcogenide $TiSe_2$ is interesting for its complex electronic properties [53,54], particularly the formation of a CDW below ∼200 K [55]. A subtle structural distortion accompanies

the CDW transition, making $TiSe_2$ a good test case for the ability to pick out small but long-range distortions in PDF data. This will be complementary to the MnTe test case, where the distortion is large but highly localized.

The CDW state in $TiSe_2$ forms a $2 \times 2 \times 2$ superlattice of the $P\bar{3}m1$ high-temperature parent structure [55]. The supercell contains 24 atoms (8 formula units) and therefore a total of 72 degrees of freedom for $P1$ symmetry, which we selected to provide the most general possible exploration of potential distortions. For each of the 72 symmetry modes, we performed a PDF fit to the 5-K data from 1.5 - 20 Å by first optimizing the lattice parameters and scale factor, then adding the symmetry-lowering mode amplitude and the displacement allowed in the parent space group ($P\bar{3}m1$), and finally adding the ADPs. To quantify the impact of each symmetry mode, we use the goodness-of-fit metric $R_w = \sqrt{\left(\sum_i \left[G_{\mathrm{obs}}(r_i) - G_{\mathrm{calc}}(r_i)\right]^2 / \sum_i G_{\mathrm{obs}}^2(r_i)\right)}$, where r_i is the i^{th} value in the r grid of the experimental data, G_{obs} is the observed PDF, and G_{calc} is the calculated PDF. A lower value of R_w indicates better agreement with the data. In Fig. 4.2(a), we plot R_w versus mode amplitude for all 72 modes tested individually, along with a horizontal line at $R_w = 0.0571$ marking the base value with no symmetry-breaking modes included. We see that most of the modes provide minimal improvement to the fit. However, two groups of modes improve the fit significantly more than the others, indicated by the arrows on the figure. These are the Ti E_u and the Se E modes of the L_1^- irrep, corresponding to in-plane distortions of the Ti and Se atoms (refer to Fig. 4.1). Each group of modes includes three equivalent distortions that are rotated 120° from each other and, given the 1D nature of the PDF data, have identical effects on the calculated PDF. The L_1^- irrep to which these modes belong is precisely the one responsible for the known CDW distortion in $TiSe_2$, which consists of equal superpositions of the three branches of the Ti E_u and the Se E modes. That the PDF fits naturally pick out these modes confirms the ability of this symmetry-motivated fitting strategy to identify even rather subtle distortions. Refinements against neutron PDF data at 100 K yielded consistent results. The fit was improved further when the same branches of the Ti and Se modes were refined together (e.g. $E_u(a)$ and $E(a)$ for Ti and Se, respectively), lowering R_w from 0.0571 to 0.0542. The corresponding fit is displayed in Fig. 4.2(c). The refined mode amplitudes at

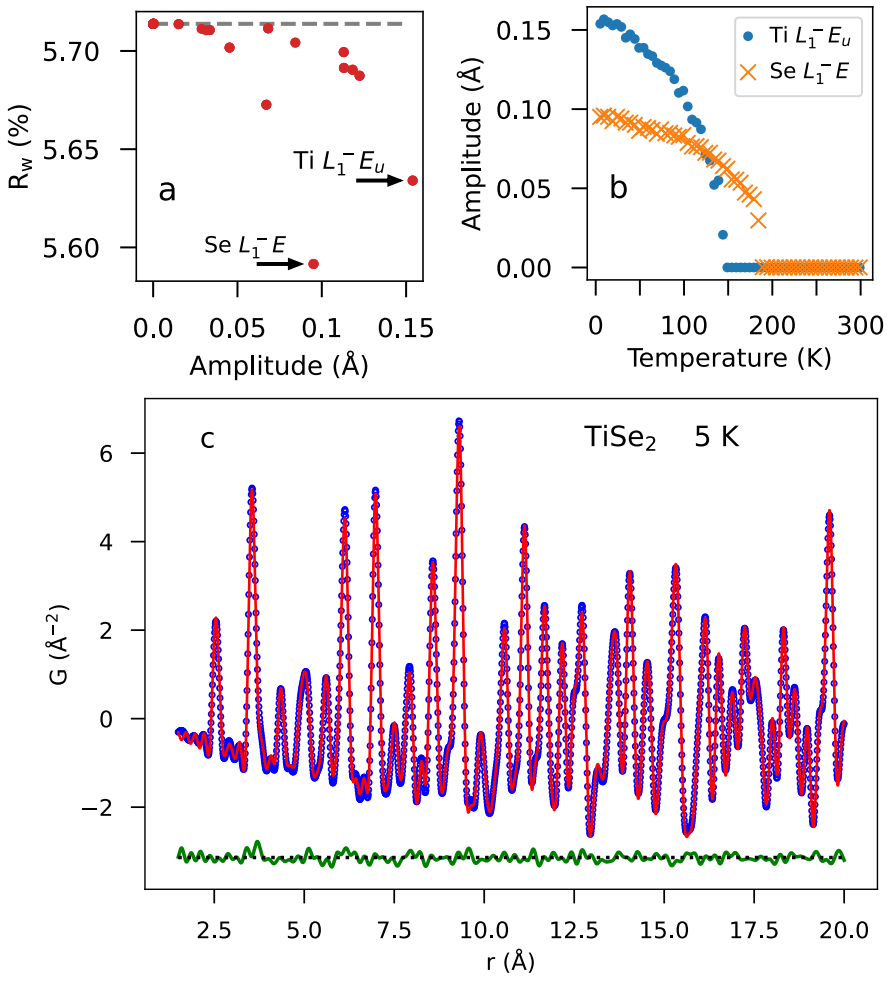

Figure 4.2 (a) A plot of R_w versus mode amplitude for the 72 distortion modes. The arrows indicate the modes that improved the fit most significantly, namely the Ti E_u and Se E modes of the L_1^- irrep. Note that 72 distinct points are not visible, because multiple modes may have the same effect on the calculated powder PDF pattern and therefore overlap on the plot. (b) Temperature dependence of the refined amplitudes of the Ti $E_u(a)$ and Se $E(a)$ modes of the L_1^- irrep. (c) A representative PDF fit to data at 5.1 K with both modes active. The blue symbols represent the experimental data, the red curve the calculated PDF, and the green curve the fit residual, offset for clarity.

5 K equate to displacements of 0.047(3) and 0.024(4) Å for Ti and Se, respectively, with the Ti-Se nearest-neighbor distance decreasing by approximately 0.05 Å. These values are close to previously published results using traditional neutron and x-ray diffraction [56, 57].

Having identified the active distortion modes at 5 K, we then performed fits to the remaining x-ray PDF data sets with the Ti $E_u(a)$ and Se $E(a)$ modes included individually to examine the temperature dependence of the distortion. As illustrated in Fig. 4.2(b), we see that the mode amplitudes decrease with increasing temperature until reaching zero between 150 and 200 K, corresponding reasonably well to the accepted CDW transition temperature around 200 K. The discrepancy in temperature may be due to the difficulty of resolving very small displacements near the transition in our data. The figure demonstrates how the mode amplitudes serve as order parameters to identify structural transitions. Interestingly, the refined Se $E(a)$ mode amplitude becomes nonzero below 190 K, while the Ti $E_u(a)$ mode amplitude does so only below about 145 K. This may indicate that the Se distortion drives the CDW transition, but it may also occur simply because the weaker scattering strength of Ti reduces the sensitivity of the fits to Ti displacements compared to Se displacements. Additional studies could provide further clarity on this.

4.4.2 MnTe

Hexagonal MnTe (space group $P6_3/mmc$) is an antiferromagnetic semiconductor that has garnered interest as a potential high-performance thermoelectric material [9, 42, 58–60] and as a platform for antiferromagnetic spintronics [61]. In the context of the present work, MnTe is a useful example because PDF analysis reveals a large short-range distortion of the local structure that exists in a wide temperature range spanning room temperature. This is manifest as a significant misfit below approximately 3.5 Å in the PDF fits when the published hexagonal structure is used [62], as shown by the circled portion of the fit residual in Fig. 4.3(a) and (b) for x-ray and neutron PDF, respectively. The data were collected at 300 K. A zoomed-in view of the misfit for the x-ray PDF pattern appears in Fig. 4.3(c), revealing that the calculated peak is off-centered relative to the observed peak. The origin and significance of this feature in the local structure will be discussed elsewhere, but the

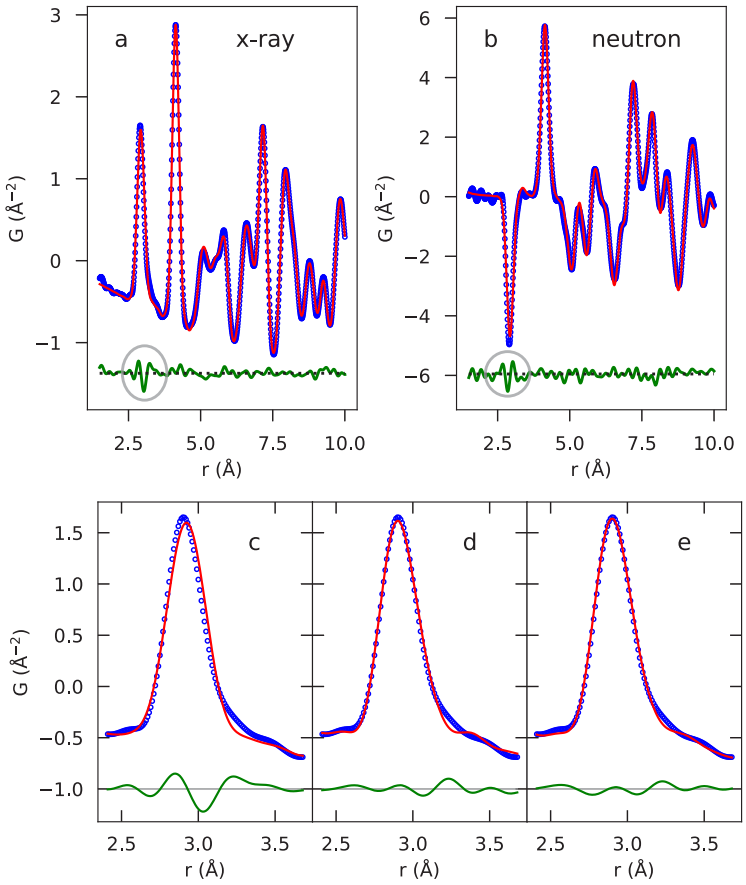

Figure 4.3 (a) X-ray PDF fit to MnTe at 300 K using the published hexagonal structure [62]. The blue symbols and red curve show the observed and calculated PDF, respectively, while the green curve shows the fit residual (offset vertically for clarity). (b) Same as (a), but for neutron PDF data (with the magnetic PDF [15, 27] included in the fit). (c) Zoomed in view of the x-ray PDF fit in panel (a) highlighting the failure of the model for the first peak. (d) Fit when the Te $E'(a)$ mode of the Γ^{5+} irrep is active. (e) Fit when the Te $E'(a)$ mode of the Γ^{5+} irrep and the Mn $E_u(a)$ mode of the Γ^{6-} irrep are active.

objective here is to demonstrate that a symmetry-driven approach can be successfully applied to highly localized structural distortions, in addition to long-range distortions such as the example given in $TiSe_2$.

To investigate the local distortion in MnTe, we systematically tested each of the 12 displacive symmetry modes in the conventional unit cell assuming $P1$ symmetry. We restricted the fit range to 1.5 – 3.75 Å, since the misfit is localized to the first large peak in the PDF pattern. To avoid over-fitting to this short data range, we fixed the lattice parameters to the values determined from a longer-range fit (1.5 – 20 Å) and optimized only a scale factor, an isotropic thermal factor for each atomic species, and the symmetry mode amplitude. The peak-sharpening parameter δ_1 was fixed to the value determined from the longer-range fit.

Of the 12 symmetry mode amplitudes, 11 had a negligible effect on the fit when tested individually. However, the Te $E'(a)$ mode of the Γ^{5+} irrep improved the fit dramatically, reducing R_w from 0.115 to 0.058 for the x-ray fit and similarly for the neutron fit. Both data sets yielded a mode amplitude corresponding to a Te displacement of $\sim$0.126(4) Å. The improved fit is shown for the x-ray data in Fig. 4.3(d); notably, the calculated peak is now centered on the experimental peak. This symmetry mode corresponds to antiparallel displacements of the two Te atoms toward the nearest face of the unit cell, as illustrated in Fig. 4.4. If this were a coherent distortion throughout the entire crystal structure, the crystallographic symmetry would be lowered to space group *Cmcm*.

Refining pairs of symmetry mode amplitudes simultaneously provides further improvement to the fit, albeit only slightly. Fig. 4.3(e), for example, shows the x-ray fit when the same Te $E'(a)$ mode of the Γ^{5+} irrep and the Mn $E_u(a)$ mode of the Γ^{6-} irrep are both active. However, other pairs of modes yielded equally good fits, indicating that the data range over which the local distortion is observed is insufficient to remove all ambiguity. Whether or not the peak-sharpening parameters δ_1 or δ_2 were included also influenced which mode pairs yielded the best fit. On the other hand, the single-mode refinements were robust against variations in the choice of δ_1 or δ_2 (or no peak-sharpening function at all), the number of unique ADPs, and the starting values of the variables, building confidence in the reliability of the single-mode results.

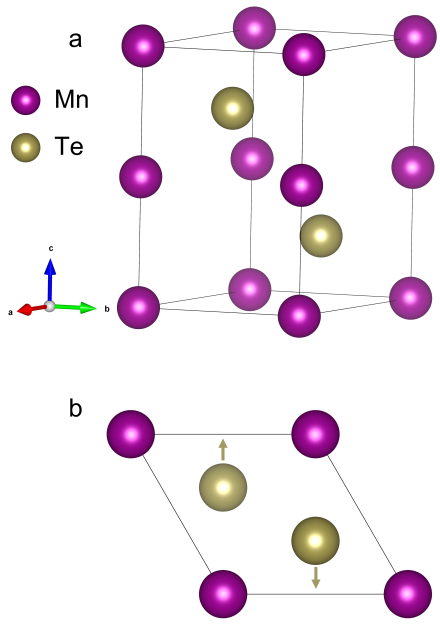

Figure 4.4 (a) Conventional unit cell of MnTe, visualized with VESTA [45]. (b) View of the unit cell looking down the c axis, with the Te displacements of the $\Gamma^{5+}E'(a)$ shown by the arrows.

4.5 Discussion and Conclusion

We demonstrated the utility of the symmetry-mode approach to fitting PDF data for two complementary use cases. In the case of $TiSe_2$, we identified a structural phase transition present over the full r range of the data in a more straightforward manner than would have been possible using traditional PDF fitting methods with xyz atomic coordinates as fit variables. The amplitudes of the active symmetry modes served as structural order parameters to show subtle but observable changes to the long-range structure, consistent with published results. Here, the advantage of the symmetry-driven methods over the traditional xyz approach is the reduced number of free parameters necessary to test and identify distorted structural models that fit the data. Only two nonzero mode amplitudes were necessary to characterize the distorted structure, while systematic testing of the individual atomic coordinates would have required a much larger number of fit variables to arrive at the same result.

The MnTe case offers a proof of concept for fitting distortions with shorter correlation lengths, as well. The distortion was only apparent in the data below about 4 Å. The flexibility of our

implementation allows for the isolation, or concurrent testing, of individual modes and groups of modes as defined by the user. For MnTe, we identified a single Te mode that resulted in a much better fit when activated. The extremely localized nature of this distortion obscures the notion of symmetry modes somewhat, but the symmetry mode basis nevertheless provided a useful parameterization, leading us to identify an in-plane distortion of the Te atoms as the likely cause of the misfit in the original fit.

A benefit of using the flexible DiffPy fitting framework is that users can customize the fitting procedure in any way they desire. For example, one could easily execute the fit multiple times with random starting values, impose a penalty to the cost function for each active symmetry mode, or set a threshold improvement value in R_w to allow a mode to be considered active. These strategies have all been suggested previously as a way to improve the reliability of exhaustive symmetry-mode testing [22, 25]. Our code can also be extended in a straightforward manner to include the rotational, occupational, and magnetic modes calculated by ISODISTORT, although that is beyond the scope of the present work. We expect that symmetry-adapted PDF analysis will become increasingly common in the field of total scattering, leading to new physical insights into the local structure of materials.

4.6 Code availability and usage

The analysis methods introduced in this work are based on fully open-source software. We have developed two new packages as part of this work: `pydistort` (https://github.com/FrandsenGroup/pydistort) for automated interactions with the ISODISTORT web-based software and `isotools` (https://github.com/FrandsenGroup/isotools) for adapting the ISODISTORT output to be compatible with the `diffpy` library [44].

For this portion of the research we thank Branton Campbell for valuable discussions regarding symmetry-adapted distortion modes and ISODISTORT. We acknowledge Brian Toby and Robert von Dreele, who developed the first python code to interface with ISODISTORT as part of their GSAS-II

program. Work by P.K.H., R.B., and B.A.F. was supported by the U.S. Department of Energy, Office of Science, Office of Basic Energy Sciences (DOE-BES) through Award No. DE-SC0021134. A.M.H. acknowledges supper from the Natural Sciences and Engineering Research Council of Canada (NSERC) and the CIFAR Azrieli Global Scholars program. J.M.M. was supported by the National Science Foundation Graduate Research Fellowship under Grant DGE 1842494. This study used resources at the Spallation Neutron Source (SNS), a DOE Office of Science User Facility operated by the Oak Ridge National Laboratory. This research used beamline 28-ID-1 of the National Synchrotron Light Source II, a U.S. Department of Energy (DOE) Office of Science User Facility operated for the DOE Office of Science by Brookhaven National Laboratory under Contract No. DE-SC0012704.

Chapter 5

Summary

Two significant extensions to PDF analysis are shown here and specifically implemented in the open-sourced `Diffpy` package. The 3D-ΔmPDF method offers a tool to compare a model structure directly to single crystal neutron diffraction and analyze the directionally dependant local magnetic structure as it deviates from the long range magnetic structure. The MnTe magnetic structure analysis shows how the 3D-ΔmPDF can be used to better understand the anisotropic magnetic correlations present in the local structure. The implementation of the magnetic structure for the sake of the computation of the 3D-ΔmPDF allows for the definition of anisotropic correlation lengths, described in detail in the appendix, which allows for a fully general definition of local correlation lengths.

In the case of the symmetry-adapted distortion method, two examples are given, as well as a detailed description of the methods and implementation of the analysis. The symmetry-apdapted fitting method offers a clear and useful analysis of the locally distorted structure, as seen in both the $TiSe_2$ case and, more subtly, in the MnTe case. Our implementation includes key tools for researchers seeking to use this technique, including a programmatic interface to the ISODISTORT package. The ISODISTORT interface tools allow for a fully algorithmic fitting routine with no need for manual interaction with a graphic user interface, facilitating efficient and thorough analysis of locally distorted structures. These two additions to the PDF analysis capabilities of `Diffpy` will facilitate ongoing research in the field of local structure effects.

Bibliography

[1] T. Egami and S. J. L. Billinge, *Underneath the Bragg peaks: structural analysis of complex materials* (Pergamon Press, Elsevier, Oxford, England, 2003).

[2] S. J. L. Billinge and I. Levin, "The problem with determining atomic structure at the nanoscale," **316,** 561–565 (2007).

[3] D. A. Keen and A. L. Goodwin, "The crystallography of correlated disorder," Nature **521,** 303–309 (2015).

[4] D. A. Keen, "A comparison of various commonly used correlation functions for describing total scattering," J. Appl. Crystallogr. **34,** 172–177 (2001).

[5] H. M. Rietveld, "A profile refinement method for nuclear and magnetic structures," J. Appl. Crystallogr. **2,** 65–71 (1969).

[6] R. A. Young, *The Rietveld Method*, *International Union of Crystallography Monographs on Crystallography* (Oxford University Press, Oxford, New York, 1995).

[7] C. A. Young and A. L. Goodwin, "Applications of pair distribution function methods to contemporary problems in materials chemistry," J. Mater. Chem. **21,** 6464–6476 (2011).

[8] M. W. Terban and S. J. L. Billinge, "Structural Analysis of Molecular Materials Using the Pair Distribution Function," Chemical Reviews **122,** 1208–1272 (2022).

[9] R. Baral *et al.*, "Real-space visualization of short-range antiferromagnetic correlations in a magnetically enhanced thermoelectric," Matter **5,** 1853–1864 (2022).

[10] B. A. Frandsen, H. K. Parker, J. A. Christensen, E. Stubben, and S. J. L. Billinge, "diffpy.mpdf: open-source software for magnetic pair distribution function analysis," **55,** 1377—1382 (2022).

[11] P. K. Hamilton, J. M. Moya, A. M. Hallas, E. Morosan, R. Baral, and B. A. Frandsen, "Symmetry-mode analysis for local structure investigations using pair distribution function data,", 2023, arXiv:2303.14484 [cond-mat].

[12] D. A. Keen and A. L. Goodwin, "The crystallography of correlated disorder," Nature **521,** 303–309 (2015).

[13] B. Frandsen, X. Yang, and S. J. L. Billinge, "Magnetic pair distribution function analysis of local magnetic correlations," Acta Crystallographica Section A: Foundations and Advances **70,** 3–11 (2014), number: 1 Publisher: International Union of Crystallography.

[14] B. A. Frandsen and S. J. L. Billinge, "Magnetic structure determination from the magnetic pair distribution function (mPDF): ground state of MnO," Acta Crystallographica Section A: Foundations and Advances **71,** 325–334 (2015), number: 3 Publisher: International Union of Crystallography.

[15] B. A. Frandsen and S. J. L. Billinge, "Magnetic structure determination from the magnetic pair distribution function (mPDF): ground state of MnO," **71,** 325–334 (2015).

[16] N. Roth, A. F. May, F. Ye, B. C. Chakoumakos, and B. B. Iversen, "Model-free reconstruction of magnetic correlations in frustrated magnets," IUCrJ **5,** 410–416 (2018).

[17] S. J. L. Billinge and M. G. Kanatzidis, "Beyond crystallography: the study of disorder, nanocrystallinity and crystallographically challenged materials," **7,** 749–760 (2004).

[18] E. Dagotto, "Complexity in strongly correlated electronic systems," Science **309,** 257–262 (2005).

[19] Y. Tokura, M. Kawasaki, and N. Nagaosa, "Emergent functions of quantum materials," Nature Phys. **13,** 1056–1068 (2017).

[20] L. Desgranges, Y. Ma, P. Garcia, G. Baldinozzi, D. Siméone, and H. E. Fischer, "Understanding Local Structure versus Long-Range Structure: The Case of UO_2," Chem.-Eur. J. **24,** 2085–2088 (2018).

[21] H. Zhu, Y. Huang, J. Ren, B. Zhang, Y. Ke, A. K.-Y. Jen, Q. Zhang, X.-L. Wang, and Q. Liu, "Bridging Structural Inhomogeneity to Functionality: Pair Distribution Function Methods for Functional Materials Development," Adv. Sci. **8,** 2003534 (2021).

[22] S. Kerman, B. J. Campbell, K. K. Satyavarapu, H. T. Stokes, F. Perselli, and J. S. O. Evans, "The superstructure determination of displacive distortions *via* symmetry-mode analysis," Acta Crystallogr. A **68,** 222–234 (2012).

[23] D. J. Gawryluk, Y. M. Klein, T. Shang, D. Sheptyakov, L. Keller, N. Casati, P. Lacorre, M. T. Fernández-Díaz, J. Rodríguez-Carvajal, and M. Medarde, "Distortion mode anomalies in bulk $PrNiO_3$: Illustrating the potential of symmetry-adapted distortion mode analysis for the study of phase transitions," Phys. Rev. B **100,** 205137 (2019).

[24] B. Campbell, H. Stokes, D. Tanner, and D. Hatch, "ISODISPLACE: An Internet Tool for Exploring Structural Distortions," J. Appl. Crystallogr. **39,** 607–614 (2006).

[25] T. A. Bird, A. Herlihy, and M. S. Senn, "Symmetry-adapted pair distribution function analysis (SAPA): a novel approach to evaluating lattice dynamics and local distortions from total scattering data," J. Appl. Crystallogr. **54,** 1514—1520 (2021).

[26] A. A. Coelho, "*TOPAS* and *TOPAS-Academic*: an optimization program integrating computer algebra and crystallographic objects written in C++," J. Appl. Crystallogr. **51,** 210–218 (2018).

[27] B. A. Frandsen, X. Yang, and S. J. L. Billinge, "Magnetic pair distribution function analysis of local magnetic correlations," **70,** 3–11 (2014).

[28] T. Egami and S. J. L. Billinge, *Underneath the Bragg peaks: structural analysis of complex materials*, 2nd ed. (Elsevier, Amsterdam, 2012).

[29] B. A. Frandsen, M. Brunelli, K. Page, Y. J. Uemura, J. B. Staunton, and S. J. L. Billinge, "Verification of Anderson Superexchange in MnO via Magnetic Pair Distribution Function Analysis and *ab initio* Theory," Phys. Rev. Lett. **116,** 197204 (2016).

[30] B. A. Frandsen, E. S. Bozin, E. Aza, A. F. Martínez, M. Feygenson, K. Page, and A. Lappas, "Nanoscale degeneracy lifting in a geometrically frustrated antiferromagnet," Phys. Rev. B **101,** 024423 (2020).

[31] B. A. Frandsen, K. A. Ross, J. W. Krizan, G. J. Nilsen, A. R. Wildes, R. J. Cava, R. J. Birgeneau, and S. J. L. Billinge, "Real-space investigation of short-range magnetic correlations in fluoride pyrochlores $NaCaCo_2F_7$ and $NaSrCo_2F_7$ with magnetic pair distribution function analysis," **1,** 074412 (2017).

[32] N. Roth, F. Ye, A. F. May, B. C. Chakoumakos, and B. B. Iversen, "Magnetic correlations and structure in bixbyite across the spin-glass transition," Phys. Rev. B **100,** 144404 (2019).

[33] E. Lefrançois *et al.*, "Spin decoupling under a staggered field in the $Gd_2Ir_2O_7$ pyrochlore," Phys. Rev. B **99,** 060401 (2019).

[34] Z. Dun *et al.*, "Neutron scattering investigation of proposed Kosterlitz-Thouless transitions in the triangular-lattice Ising antiferromagnet $TmMgGaO_4$," Phys. Rev. B **103,** 064424 (2021).

[35] Y. Zhang, T. Scholz, R. Dronskowski, M. T. McDonnell, and M. G. Tucker, "Local magnetic cluster size identified by neutron total scattering in the site-diluted spin glass $Sn_xFe_{4-x}N$ (x = 0.88)," Phys. Rev. B **100,** 014419 (2019).

[36] B. A. Frandsen, Z. Gong, M. W. Terban, S. Banerjee, B. Chen, C. Jin, M. Feygenson, Y. J. Uemura, and S. J. L. Billinge, "Local atomic and magnetic structure of dilute magnetic semiconductor $(Ba,K)(Zn,Mn)_2As_2$," Phys. Rev. B **94,** 094102 (2016), selected as Editors' Suggestion.

[37] K. Kodama, K. Ikeda, S.-i. Shamoto, and T. Otomo, "Alternative Equation on Magnetic Pair Distribution Function for Quantitative Analysis," J. Phys. Soc. Jpn **86,** 124708 (2017).

[38] M. Tripathi, T. Chatterji, H. E. Fischer, R. Raghunathan, S. Majumder, R. J. Choudhary, and D. M. Phase, "Role of local short-scale correlations in the mechanism of negative magnetization," Phys. Rev. B **99,** 014422 (2019).

[39] T. Weber and A. Simonov, "The three-dimensional pair distribution function analysis of disordered single crystals: basic concepts," Z. Kristallogr. **227,** 238–247 (2012).

[40] J. Weng, E. D. Dill, J. D. Martin, R. Whitfield, C. Hoffmann, and F. Ye, "K-space algorithmic reconstruction (KAREN): a robust statistical methodology to separate Bragg and diffuse scattering," J. Appl. Crystallogr. **53,** 159–169 (2020).

[41] N. Kunitomi, Y. Hamaguchi, and S. Anzai, "Neutron diffraction study on manganese telluride," J. Phys.-Paris **25,** 568–574 (1964).

[42] Y. Zheng *et al.*, "Paramagnon drag in high thermoelectric figure of merit Li-doped MnTe," Sci. Adv. **5,** eaat9461 (2019).

[43] R. Baral *et al.*, "Real-space visualization of short-range antiferromagnetic correlations in a magnetically enhanced thermoelectric," Matter **5,** 1853–1864 (2022).

[44] P. Juhás, C. L. Farrow, X. Yang, K. R. Knox, and S. J. L. Billinge, "Complex Modeling: a strategy and software program for combining multiple information sources to solve ill-posed structure and nanostructure inverse problems," **71,** 562–568 (2015).

[45] K. Momma and F. Izumi, "VESTA 3 for three-dimensional visualization of crystal, volumetric and morphology data," J. Appl. Crystallogr. **44,** 1272–1276 (2011).

[46] B. H. Toby and R. B. Von Dreele, "*GSAS-II*: the genesis of a modern open-source all purpose crystallography software package," J. Appl. Crystallogr. **46,** 544–549 (2013).

[47] A. P. Cracknell, S. C. Miller, W. F. Love, and B. L. Davies, *Kronecker product tables. Vol. 1, General introduction and tables of irreducible representations of space groups* (IFI/Plenum Data Company, New York, 1979), oCLC: 1055649799.

[48] J. M. Moya, C.-L. Huang, J. Choe, G. Costin, M. S. Foster, and E. Morosan, "Effect of synthesis conditions on the electrical resistivity of $TiSe_2$," Phys. Rev. Materials **3,** 084005 (2019).

[49] C. Prescher and V. B. Prakapenka, "DIOPTAS: a program for reduction of two-dimensional X-ray diffraction data and data exploration," High Pressure Res. **35,** 223–230 (2015).

[50] X. Yang, P. Juhás, C. Farrow, and S. J. L. Billinge, "xPDFsuite: an end-to-end software solution for high throughput pair distribution function transformation, visualization and analysis," (2015), 1402.3163.

[51] J. Neuefeind, M. Feygenson, J. Carruth, R. Hoffmann, and K. K. Chipley, "The Nanoscale Ordered MAterials Diffractometer NOMAD at the Spallation Neutron Source SNS," Nucl. Instrum. Meth. B **287,** 68 – 75 (2012).

[52] M. McDonnell, D. Olds, K. Page, J. Neuefeind, M. Tucker, J. Bilheux, W. Zhou, and P. Peterson, "ADDIE: ADvanced DIffraction Environment – A Software Environment for Analyzing Neutron Diffraction Data," Acta Crystallogr. A **73,** a377 (2017).

[53] S. Manzeli, D. Ovchinnikov, D. Pasquier, O. V. Yazyev, and A. Kis, "2D transition metal dichalcogenides," Nature Reviews Materials **2,** 1–15 (2017), number: 8 Publisher: Nature Publishing Group.

[54] X. Yin, C. S. Tang, Y. Zheng, J. Gao, J. Wu, H. Zhang, M. Chhowalla, W. Chen, and A. T. S. Wee, "Recent developments in 2D transition metal dichalcogenides: phase transition and applications of the (quasi-)metallic phases," Chemical Society Reviews **50,** 10087–10115 (2021), publisher: The Royal Society of Chemistry.

[55] F. J. Di Salvo, D. E. Moncton, and J. V. Waszczak, "Electronic properties and superlattice formation in the semimetal ${\mathrm{TiSe}}_{2}$," Physical Review B **14,** 4321–4328 (1976), publisher: American Physical Society.

[56] F. J. Di Salvo, D. E. Moncton, and J. V. Waszczak, "Electronic properties and superlattice formation in the semimetal $TiSe_2$," Phys. Rev. B **14,** 4321–4328 (1976).

[57] X.-Y. Fang, H. Hong, P. Chen, and T.-C. Chiang, "X-ray study of the charge-density-wave transition in single-layer $TiSe_2$," Phys. Rev. B **95,** 201409 (2017).

[58] Y. Xu, W. Li, C. Wang, J. Li, Z. Chen, S. Lin, Y. Chen, and Y. Pei, "Performance optimization and single parabolic band behavior of thermoelectric MnTe," J. Mater. Chem. A **5,** 19143–19150 (2017).

[59] Y. Ren, J. Yang, Q. Jiang, D. Zhang, Z. Zhou, X. Li, J. Xin, and X. He, "Synergistic effect by Na doping and S substitution for high thermoelectric performance of p-type MnTe," J. Mater. Chem. C **5,** 5076–5082 (2017).

[60] J. Dong, C.-F. Wu, J. Pei, F.-H. Sun, Y. Pan, B.-P. Zhang, H. Tang, and J.-F. Li, "Lead-free MnTe mid-temperature thermoelectric materials: facile synthesis, p-type doping and transport properties," J. Mater. Chem. C **6,** 4265–4272 (2018).

[61] D. Kriegner *et al.*, "Multiple-stable anisotropic magnetoresistance memory in antiferromagnetic MnTe," Nat. Commun. **7,** 11623 (2016).

[62] J. E. D'Sa, P. Bhobe, K. Priolkar, A. Das, S. Paranjpe, R. Prabhu, and P. Sarode, "Low-temperature neutron diffraction study of MnTe," J. Magn. Magn. Mater. **285,** 267–271 (2005).